pp 60–86.
doi:10.1017/aer.2020.79

Energy acquisition of a small solar UAV using dynamic soaring

S. Liu
763813367@qq.com
School of Aeronautics
Northwestern Polytechnical University
Xi'an
China

J. Bai
junqiang@nwpu.edu.cn
School of Aeronautics
Northwestern Polytechnical University
Xi'an
China

C. Wang
Chang'an University
Xi'an
China

ABSTRACT

Dynamic soaring improves the endurance of Unmanned Aerial Vehicles (UAVs) by obtaining energy from the horizontal wind shear gradient. The use of dynamic soaring in small solar UAVs can mitigate the trade-off between energy capacity and battery weight to achieve continuous all-day flight. The goal of this study is to determine the optimal energy acquisition methods for small solar UAVs using dynamic soaring and to decrease the battery weight to achieve all-day flight. A dynamic soaring UAV model that considers the influence of the wind shear gradient and a solar power energy model are established. The conditions to obtain a closed-loop energy system during daytime and nighttime flights are discussed, and the minimum mass of the energy system required for these conditions is determined. Simulations of single-cycle circular flights and a 72-h continuous flight of a small solar UAV are performed. The analyses and simulation results show that: (1) the combination of dynamic soaring and solar technology significantly reduces the energy consumption and reduces the required battery weight, (2) the flight speed and flight attitude angles have significant effects on the optimal total energy acquisition and (3) wind fields with a large horizontal gradient and strong solar illumination provide energy and load advantages.

Received 30 March 2020; revised 10 June 2020; accepted 27 July 2020.

Keywords: dynamic soaring; small solar UAV; energy acquisition; trajectory optimisation; solar energy

NOMENCLATURE

AR	aspect ratio
b	wingspan
C_L	lift coefficient
C_D	drag coefficient
C_{D0}	parasitic drag coefficient
D	drag
E	energy
h	flight altitude
H_R	reference height
I	solar constant
I_0	vertical solar illumination intensity
K_D	induced drag factor
L	lift
M	number of nodes
m	mass
nd	number of days in a year
$\mathbf{n_s}$	vector of the earth–sun direction
$\mathbf{n_w}$	normal vector of the wing
P	power; energy change per time
p	intensity of the wind field gradient
S_w	wing area
$t_{mission}$	the time of the mission
$\mathbf{u}$	input control vector
V	airspeed
V_R	wind speed at reference height
V_W	wind speed
$\mathbf{x}$	state vector of the system
β_s	solar elevation angle
ε	eccentricity of the earth
η_{asc}	ratio of the area of the solar panels to the wing area
η_{sc}	energy conversion efficiency of the solar panels
η_T	efficiency of the propulsion system
η_m	efficiency of the energy management system
γ	pitch angle
γ_s	solar azimuth
κ_{bat}	battery energy density
μ	bank angle
ω_s	sun hour angle

https://doi.org/10.1017/aer.2020.79 Published online by Cambridge University Press

ψ heading angle
σ_T power weight ratio of propulsion system
θ_s geographical latitude of the flight location
φ_s declination angle
ξ_T power output factor of the propulsion system

Subscripts

sp solar power system
T propulsion system
bat battery
max maximum
D drag

1.0 INTRODUCTION

A solar aircraft uses solar power as its main energy source and has better endurance and mission sustainability than other types of aircraft; therefore, solar aircraft research is being conducted worldwide. UAVs offer prominent advantages for reconnaissance and surveillance tasks[1,2], and they are already being operated by military forces and civilian organisations[3,4]. Small solar UAVs are less costly than larger UAVs; however, due to load limitations, the on-board energy capacity is relatively low[5], limiting their practical applications. Long-endurance flight is a key design objective of aircraft, and all-day flight is a long-term goal in solar vehicle design[6,7]. However, due to the contradiction between battery weight and energy capacity limitations[8], small solar UAVs have difficulty achieving all-day flight.

Numerous studies have been conducted to extend the flight duration of solar UAVs and achieve all-day flight. Klesh and Kabamba[9] focused on maximising the energy ratio and found that the range of solar-powered UAVs could be increased by efficient design and optimal path planning. Sineglazov et al. developed a power–energy system for energy management[10,11]. Spangelo et al.[12,13] investigated the relationship between the flight trajectory and energy acquisition efficiency for a vertical cylindrical surface, and the effects of the flight path angle and heading angle were analysed. Chang et al.[14,15] used active rotation of photovoltaic modules to obtain more solar energy. In these studies, the efficiency of the solar energy acquisition was improved by adjusting the flight trajectory, flight attitude and energy management, but the energy loss at night when there is no solar energy was not addressed. Research on the constraint of energy on-board still needs to be done.

Other research has focused on energy consumption reduction. Brandt and Gilliamt[16] proposed the concept of storing gravitational potential energy. Ma Dongli et al. analysed the effect of the flight trajectory of solar aircraft at different flight altitudes[17]. In these studies, the energy consumption was reduced at night, but the efficiency of solar energy acquisition during the day was not addressed.

An additional onboard energy source is needed to improve energy acquisition during the day and reduce energy consumption at night. Therefore, the dynamic soaring technique is investigated in this study. All-day flight of small solar UAVs can be achieved by obtaining additional energy from the wind field.

Dynamic soaring is a technique for extending the flight duration and allows small UAVs to obtain energy from a horizontal wind gradient using flight manoeuvres. Lord Rayleigh analysed the flight pattern of albatrosses and proposed the theory of dynamic soaring[18].

https://doi.org/10.1017/aer.2020.79 Published online by Cambridge University Press

According to Sachs et al., drifting albatrosses use dynamic soaring to gain extra energy from the wind field. The birds can fly continuously from South Georgia to the Southwest Pacific with a flight power of 81 W in 13.2 days. The energy they consume is equivalent to 5.6–11.9 L of gasoline, far exceeding their energy reserves[19]. Horizontal wind field gradients are ubiquitous at the altitudes commonly used by small UAVs. With appropriate path planning and flight manoeuvres, the combination of dynamic soaring and solar energy technology can overcome the shortcomings of solar energy systems, which do not provide energy at night, and improve the energy acquisition efficiency during the day. The combination of these two energy acquisition techniques can reduce energy consumption and battery weight and allow small UAVs to achieve long-duration flight. Dynamic soaring is also available in high altitude, but due to the heavy structure and high flight speed of high-altitude solar UAVs, the energy acquisition rate provided by dynamic soaring is limited. This research mainly focusses on small solar UAV to analyse optimal energy acquisition methods.

In recent years, dynamic soaring techniques have been developed. Zhao used NPSOL to optimise the minimum energy consumption of dynamic soaring vehicles[20,21]. Sachs determined the minimum gradient wind field needed for dynamic soaring of powerless gliders[22,23]. Deittert et al. studied optimisation of the flight path to minimise the energy consumption of small UAVs using dynamic soaring[24]. Liu Duoneng et al. used the Runge–Kutta integral method to optimise dynamic soaring flight trajectories of different types of travelling and loitering patterns[25].

Zhu Bingjie analysed the energy variations during dynamic soaring flight using the Gauss pseudospectral method[26]. The use of a single type of energy has limited applications for small UAVs, whereas the combination of different energy acquisition technologies shows greater promise. Gao Xianzhong analysed the advantage of combining solar energy, dynamic soaring and gravitational potential; the benefits of dynamic soaring were preliminary discussed, but further research is needed[27].

The objectives of this study are to combine dynamic soaring with solar energy acquisition, determine the optimal energy acquisition methods for small solar UAVs using dynamic soaring and decrease the battery load to achieve all-day flight. A periodic loitering pattern is chosen to analyse the total energy change in the simulation[20]. Analyses and flight simulations of small solar UAVs using dynamic soaring are conducted to demonstrate the following: (1) the use of dynamic soaring significantly reduces the energy consumption after optimisation, and the battery weight is significantly lower when dynamic soaring is used; (2) the flight speed and flight attitude angles have significant effects on the optimal total energy acquisition; (3) the wind field shape and solar conditions have considerable effects on the ability of the solar UAV to exploit dynamic soaring for all-day flight.

2.0 MODELLING

Modelling is used to analyse the energy acquisition from the wind field and the influence of solar illumination. The models include a wind field model, a model of the solar power energy system and a flight dynamics model. The models are used to determine the energy acquisition from the horizontal wind gradient, the energy acquisition and conversion of solar radiation energy, the changes in the flight attitude and the energy expenditure during the flight.

2.1 Wind field model

Horizontal wind gradients occur widely in the atmosphere and are most common at altitudes at sea level, which is the common flying height of small UAVs. An exponential wind shear

https://doi.org/10.1017/aer.2020.79 Published online by Cambridge University Press

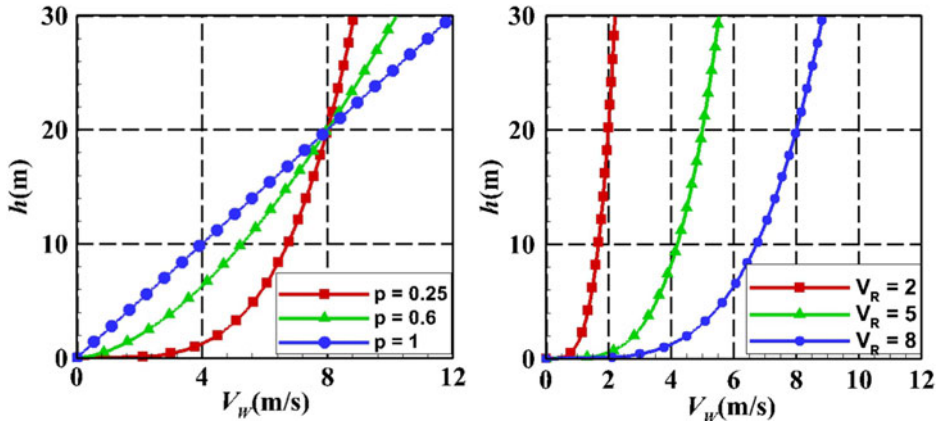

Figure 1. Wind field model with different values of p or V_R.

model is used to describe the wind field, with a horizontal gradient that is used as the energy source for dynamic soaring[19]:

$$V_W(h) = V_R\left(\frac{h}{H_R}\right)^p \quad \ldots(1)$$

where H_R and V_R represent the reference height and the wind speed at this height, respectively, h is the altitude, V_W is the wind speed at altitude h, and p is the power-law exponent, which reflects the intensity of the wind field gradient. Different values are used for different environmental conditions. Deittert chose $p = 0.143$ to describe the horizontal wind gradient above a water surface[24], and Liu Duoneng chose $p = 0.25$ for a long-term flight mission over complex terrain[26]. The default wind field value $H_R = 20$m, $p = 0.25$ and $V_R = 8$m/s are used in the simulation for a persistent wind field on land in the mid-latitude area of the Northern Hemisphere[26]. Wind fields with different parameters p and V_R are also discussed in this paper. The wind fields with different parameters are shown in Fig. 1.

In the flight simulation, we assume that the wind direction is the $+X$ direction of the earth's axis to control variables. The wind direction changes at different times of the year, but considering the terrain and other factors, the wind direction can still be considered to be in the same direction in a local environment.

2.2 Model of the solar power energy system

The model of the solar power energy system describes the solar energy acquisition and the energy output of the propulsion system. The vertical solar illumination intensity I_0 is modelled as follows[17,28,29]:

$$I_0 = I\left(\frac{1+\varepsilon\cos\alpha_s}{1-\varepsilon^2}\right)^2$$
$$\alpha_s = 2\pi(\mathrm{nd}-4)/365 \quad \ldots(2)$$

where I is the solar constant, which is 1367W/m^2, ε is the eccentricity of the earth (0.017) and nd is the number of days in a year, beginning on January 1. The vector of the earth–sun direction is $\mathbf{n_s}$:

https://doi.org/10.1017/aer.2020.79 Published online by Cambridge University Press

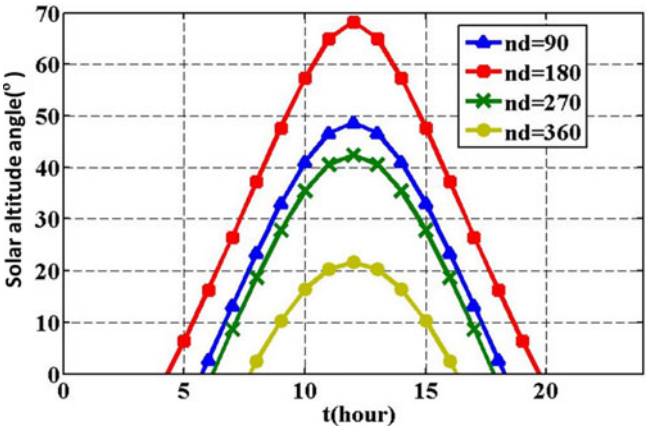

Figure 2. The solar altitude angle on different dates.

$$\begin{aligned}
\sin\beta_s &= \sin\theta_s \sin\varphi_s + \cos\theta_s \cos\varphi_s \cos(\omega_s) \\
\sin\gamma_s &= \frac{\sin\beta_s \sin\theta_s - \sin\varphi_s}{\cos\beta_s \cos\theta_s} \\
\varphi_s &= 23.45\pi \sin\left(2\pi \times \frac{284+nd}{365}\right)/180 \\
\omega_s &= \pi - \pi t_{mission}/12 \\
\mathbf{n_s} &= (\cos\beta_s \sin\gamma_s, \cos\beta_s \cos\gamma_s, \sin\beta_s)
\end{aligned} \quad \ldots (3)$$

where β_s is the solar elevation angle, γ_s is the solar azimuth measured clockwise from east, φ_s is the declination angle, θ_s is the geographical latitude of the flight location, ω_s is the sun hour angle and $t_{mission}$ is the time of the mission. The solar altitude angle on different dates is shown in Fig. 2.

The efficiency of solar energy acquisition depends on the angle between the vector of the earth–sun direction $\mathbf{n_s}$ and the normal vector of the wing $\mathbf{n_w}$:

$$P_{sun0} = I_0 \cos\langle \mathbf{n_s}, \mathbf{n_w} \rangle \quad \ldots (4)$$

The solar energy is converted to mechanical energy using the solar power energy system:

$$P_{sun} = P_{sun0} S_w \eta_{sc} \eta_{asc} \eta_m \eta_T \quad \ldots (5)$$

where S_w is the wing area, η_{asc} is the ratio of the area of the solar panels to the wing area, η_{sc} is the energy conversion efficiency of the solar panels, η_T is the efficiency of the propulsion system and η_m is the efficiency of the energy management system.

2.3 Flight dynamics model

A three-degree-of-freedom model of the UAV is adopted[20]. The sideslip angle is ignored to simplify the model and focus on the influence of dynamic soaring on the energy acquisition

https://doi.org/10.1017/aer.2020.79 Published online by Cambridge University Press

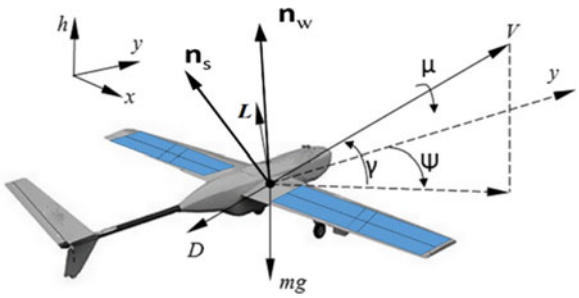

Figure 3. Forces and angles acting on the UAV.

of small solar UAVs[22,24,26]. The lift L and drag D are calculated using a simplified model as follows:

$$\begin{aligned} L &= \rho S_w C_L V^2/2 \\ D &= \rho S_w C_D V^2/2 \\ C_D &= C_{D0} + K_D C_L^2 \end{aligned} \quad \ldots(6)$$

where C_L is the lift coefficient and C_D is the drag coefficient; C_D depends on C_L, C_{D0} is the parasitic drag coefficient and K_D is the induced drag factor.

The definition of the forces and angles used in the flight model of the dynamic soaring simulation of the UAV is shown in Fig. 3.

The dynamic soaring flight model of the UAV is defined in Equation (7), which shows the changes in the flight state and position of the UAV during dynamic soaring.

$$\begin{aligned} m\dot{V} &= T - D - mg\sin\gamma - m\dot{V}_W \cos\gamma \sin\psi \\ mV\cos\gamma\dot{\psi} &= L\sin\mu - m\dot{V}_W \cos\psi \\ mV\dot{\gamma} &= L\cos\mu + m\dot{V}_W \sin\gamma\sin\psi - mg\cos\gamma \\ \dot{h} &= V\sin\gamma \\ \dot{x} &= V\cos\gamma\sin\psi + V_W \\ \dot{y} &= V\cos\gamma\cos\psi \end{aligned} \quad \ldots(7)$$

The equation is defined in the flightpath axis system, where ψ is the heading angle, γ is the pitch angle of the flight path and μ is the bank angle. The pitch angle is positive when climbing upward, and the heading angle is positive when deflecting from the positive direction of the $+Y$ axis to the the $+X$ axis, both of which are defined in the flightpath axis system. These parameters define how the flight attitude changes during dynamic soaring. (x, y, h) describes the position of the UAV in an earth-fixed reference frame, V is the airspeed and V_W is the wind speed; the wind direction is always in the x-axis direction. The lift L, drag D and thrust T are defined in the wind axis system. The variables in the kinematic formula are defined in the earth axis system.

One of the glider models that is commonly used in dynamic soaring simulations is chosen in this study[24,26]. The parameters are shown in Table 1[15,17]:

https://doi.org/10.1017/aer.2020.79 Published online by Cambridge University Press

Table 1
Model reference parameter of a small UAV

Parameter	Value	Parameter	Value
$m(kg)$	5.443	$b(m)$	4.32
$s_w(m^2)$	0.957	c_{Do}	0.017
k_D	0.0192	AR	19.54
C_{Lmax}	1.5	$\mu_{max}(^\circ)$	60
η_{asc}	0.2	η_{sc}	0.8
η_T	0.95	η_m	0.72
$\kappa_{bat}(Wh/kg)$	200	ξ_T	2.5
$\sigma_T(W/kg)$	400		

3.0 ENERGY ANALYSIS

It is necessary to limit the energy use of the aircraft to balance the energy acquisition and expenditure and ensure that the aircraft can fly day and night; therefore, closed-loop energy analysis is conducted. Analyses of the energy expenditure needed to maintain flight, the relationship between the energy acquisition and the flight attitude, the energy conditions needed for ultra-long flight and the load cost of the closed-loop energy system are also carried out.

3.1 Closed-loop energy system

The solar power energy system manages the solar energy acquisition, storage and output. The amount of energy E_{sp} changes as a result of the acquisition of solar energy E_{sun} and the energy output by the propulsion system E_T. E_{sp} is expressed as

$$E_{sp} = E_{sun} - E_T \quad \ldots (8)$$

The solar energy power system of the aircraft must be a closed-loop system to achieve all-day flight. During the day, solar radiation is absorbed and converted into electrical energy by the solar power energy system, while the system outputs energy to propel the aircraft and excess energy is stored in the batteries. At night, there is no solar radiation, and the energy output required for flight is provided by the batteries. A closed-loop energy system must be used to achieve continuous flight day and night. In the daytime, the energy converted from solar radiation by the solar cells should be greater than the energy consumption for flight, and the extra energy stored in the battery is used to maintain flight during the night. This process is called the daytime closed-loop energy process. At night, the residual energy in the battery should be no less than the energy required for night flight. This process is called the nighttime closed-loop energy process. Both processes together are called the all-day closed-loop energy process, which is expressed in Equation (9) and Fig. 4.

$$\begin{aligned} E_{wholeday} &\geq E_{need\_day} + E_{ch\arg e} \\ &= E_{sun} - E_{T\_day} + E_{ch\arg e} \\ E_{ch\arg e} &\geq E_{need\_night} = E_{T\_night} \end{aligned} \quad \ldots (9)$$

https://doi.org/10.1017/aer.2020.79 Published online by Cambridge University Press

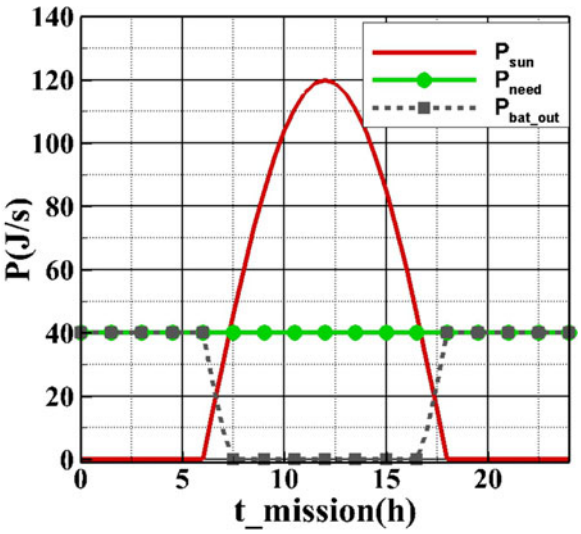

Figure 4. Sketch of all-day energy change.

In this study, we focus on a loitering flight pattern; therefore, the system has to be a closed-loop system with regard to mechanical energy. The mechanical energy $E_{mechnical}$ is defined as follows:

$$E_{mechnical} = mgh + \frac{1}{2}mV^2 \quad \ldots(10)$$

The time derivative of the mechanical energy is expressed as

$$\dot{E}_{mechnical} = mg\left(\dot{h} + \frac{1}{g}V\dot{V}\right) \quad \ldots(11)$$

The parameters in this equation are defined as

$$\dot{h} = V\sin\gamma \quad \ldots(12)$$

$$\dot{V}_W = \frac{dV_W}{dh}\dot{h} \quad \ldots(13)$$

We combine Equations (7), (12), (13) and (10) to obtain

$$\dot{E}_{mechnical} = -\frac{dV_W}{dh}mV^2\sin\gamma\cos\gamma\sin\psi + TV - DV \quad \ldots(14)$$

Equation (14) represents the changes in mechanical energy during the flight. The path of dynamic soaring is shown in Fig. 5. The right-hand side of the equation represents the wind energy obtained from dynamic soaring P_{wind}, the energy output of the propulsion system P_T and the energy consumption to overcome the resistance of aerodynamic drag P_D. When

https://doi.org/10.1017/aer.2020.79 Published online by Cambridge University Press

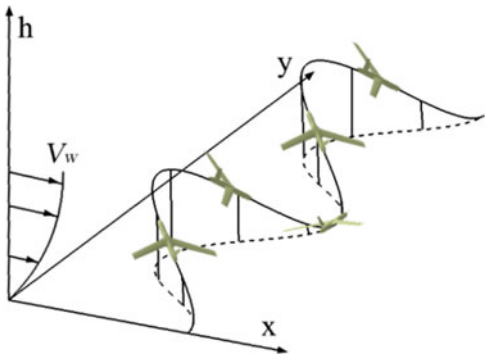

Figure 5. Path of dynamic soaring.

$\sin\gamma \sin\psi < 0$, i.e. when the UAV climbs upwind or dives downwind, then $P_{wind} > 0$, and the UAV gains energy from the wind field; otherwise, the UAV loses energy. Therefore, using appropriate flight control and path planning, the UAV represents a closed-loop energy system that does not consume mechanical energy, thereby improving its endurance.

The expression of mechanical energy is provided in Equation (15)

$$\begin{aligned} E_{mechnical} &= \int_0^{t_n} (P_{wind} - P_D + P_T)dt \\ &= E_{wind} - E_D + E_T \end{aligned} \quad \ldots (15)$$

The energy storage capacity of the solar power energy system is the primary factor that prevents a small solar UAV from meeting closed-loop conditions. The expression of the energy storage capacity is as follows:

$$E_{charge} = E_{sp\_\max} \le \eta_m \eta_T m_{bat} \kappa_{bat} \quad \ldots (16)$$

where m_{bat} is the mass of the battery and κ_{bat} is the battery energy density. After satisfying the closed-loop energy conditions, all-day flight can be achieved. In the daytime, dynamic soaring is used to charge the battery in conjunction with solar energy, whereas at night, it becomes the only external energy source to decrease the consumption of the energy stored in the battery. When the total energy output at night is less than the battery storage, the closed-loop energy conditions are met, which is expressed as:

$$\begin{aligned} P_{bat\_out} &= P_{need} - P_{sun} - P_{wind} \\ P_{bat\_out} &\ge 0 \\ P_{need} &= P_D \end{aligned} \quad \ldots (17)$$

where P_{need} is the power required for flight and P_{bat_out} is the battery power output.

3.2 Minimum mass required for power energy systems

The minimum mass of the solar power energy system, m_{sp}, is used as the evaluation index to determine the energy efficiency of the small solar UAV using dynamic soaring in a closed-loop

https://doi.org/10.1017/aer.2020.79 Published online by Cambridge University Press

energy system. The expression for m_{sp} is

$$m_{sp} = m_{sp0} + m_{bat} + m_p \quad \ldots(18)$$

The components of the mass of the solar power energy system include the battery mass m_{bat}, the power system mass m_p and the other mass m_{sp0}. The weight of the battery is an important part of the solar power energy system, and it is also the part that is most affected by dynamic soaring. The calculation function is obtained from Ref. 10.

$$\begin{aligned} m_{bat} &= \frac{E_{ch\arg e}}{\eta_m \eta_T \kappa_{bat}} = \frac{P_{T\_night} t_{night}}{\eta_m \eta_T \kappa_{bat}} \\ m_p &= \frac{P_{T\_\max} \xi_T}{\eta_T \sigma_T} \end{aligned} \quad \ldots(19)$$

A smaller m_{sp} indicates that the small solar UAV can carry a larger mission load in one mission, or complete the same mission with less energy consumption because more energy is acquired due to energy sources external to the UAV.

3.3 Analysis of optimal energy acquisition methods

The energy analysis in Equation (14) shows that most of the energy required during the flight of the small UAV comes from the energy E_{wind} obtained by dynamic soaring from the wind field gradient and the solar energy E_{sun} obtained by the solar power energy system. The energy acquisition is related to the flight attitude; therefore, the amount of energy can be maximised by adjusting the flight attitude of the aircraft.

The power corresponding to the energy obtained by dynamic soaring P_{wind} can be expressed as

$$\begin{aligned} P_{wind} &= -\frac{dV_W}{dh} mV^2 \sin\gamma \cos\gamma \sin\psi \\ &= -\frac{1}{2}\frac{dV_W}{dh} mV^2 \sin 2\gamma \sin\psi \end{aligned} \quad \ldots(20)$$

Equation (20) shows that the wind energy acquisition is related to the heading angle and flight path angle. P_{wind} is positive during upwind climbing and downwind diving, thus wind energy is acquired; in the opposite conditions, energy is expended. When $\psi = 90°, \gamma = -45°$ or $\psi = -90°, \gamma = 45°$, the aircraft can maximise the energy acquisition from the wind gradient when the aircraft is flying downwind at a 45° angle or upwind at an angle of 45°. The maximum power P_{wind} is

$$\max(P_{wind}) = \frac{1}{2}\frac{dV_W}{dh} mV^2 \quad \ldots(21)$$

In this condition, the wind energy acquisition is related to the wind gradient and flight speed. According to the actual flight conditions of a small UAV, when $dV_W/dh = 0.2s^{-1}$, $V = 21m/s$, the relationship between the wind energy acquisition and flight attitude can be obtained in Fig. 6:

There are two maximum value points of wind energy acquisition, corresponding to the two cases in the previous analysis, as well as two minimum value points, namely the points of

https://doi.org/10.1017/aer.2020.79 Published online by Cambridge University Press

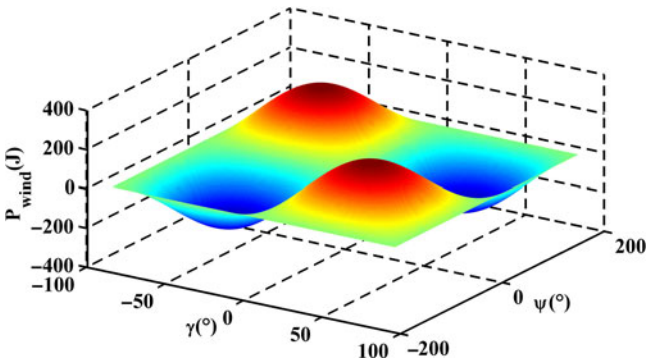

Figure 6. Relationship between wind energy acquisition and flight attitude.

upwind diving and downwind climbing. These points are in agreement with the results of the analysis of P_{wind}.

The expression for the solar energy acquisition is then

$$\begin{aligned} P_{sun} &= I_1 \cos\langle \mathbf{n_s}, \mathbf{n_w}\rangle \\ I_1 &= I_0 S_w \eta_{sc} \eta_{asc} \eta_m \eta_T \end{aligned} \quad \ldots (22)$$

where

$$\begin{aligned} \mathbf{n_s} &= (\cos\beta_s \sin\gamma_s, \cos\beta_s \cos\gamma_s, \sin\beta_s) = (\mathrm{n_{s1}}, \mathrm{n_{s2}}, \mathrm{n_{s3}}) \\ \mathbf{n_w} &= \begin{pmatrix} \sin\mu\cos\psi - \sin\gamma\cos\mu\sin\psi, \\ -\sin\mu\sin\psi - \sin\gamma\cos\mu\cos\psi, \\ \cos\mu\cos\gamma \end{pmatrix}^T \end{aligned} \quad \ldots (23)$$

The expression $\cos\langle \mathbf{n_s}, \mathbf{n_w}\rangle$ can be expanded as follows:

$$\begin{aligned} \cos\langle \mathbf{n_s}, \mathbf{n_w}\rangle &= (\sin\mu\cos\psi - \sin\gamma\cos\mu\sin\psi)\mathrm{n_{s1}} \\ &\quad + (-\sin\mu\sin\psi - \sin\gamma\cos\mu\cos\psi)\mathrm{n_{s2}} + \cos\mu\cos\gamma\,\mathrm{n_{s3}} \\ &= (\cos\psi\,\mathrm{n_{s1}} - \sin\psi\,\mathrm{n_{s2}})\sin\mu \\ &\quad + (-\sin\gamma\sin\psi\,\mathrm{n_{s1}} - \sin\gamma\cos\psi\,\mathrm{n_{s2}} + \cos\gamma\,\mathrm{n_{s3}})\cos\mu \\ &= A\sin\mu + B\cos\mu \end{aligned} \quad \ldots (24)$$

When the bank angle is a free variable in the formula, $\cos\langle \mathbf{n_s}, \mathbf{n_w}\rangle$ reaches its maximum when $\sin\mu = A/\sqrt{A^2+B^2}$:

$$\begin{aligned} \max(\cos\langle \mathbf{n_s}, \mathbf{n_w}\rangle) &= \sqrt{A^2+B^2} \\ &= \sqrt{(\cos\psi\,\mathrm{n_{s1}} - \sin\psi\,\mathrm{n_{s2}})^2 + (-\sin\gamma(\sin\psi\,\mathrm{n_{s1}} + \cos\psi\,\mathrm{n_{s2}}) + \cos\gamma\,\mathrm{n_{s3}})^2} \end{aligned} \quad \ldots (25)$$

We use the flight date $nd = 180$ and the flight time $t_{mission} = 12{:}00$ as examples, $I_1 = 553.8J$. The relationship between the solar energy acquisition and the flight attitude is shown in Fig. 7.

https://doi.org/10.1017/aer.2020.79 Published online by Cambridge University Press

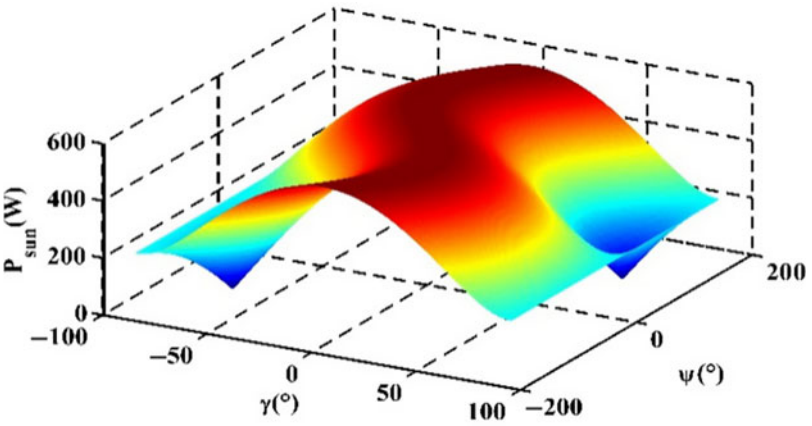

Figure 7. Relationship between solar energy acquisition and flight attitude.

The maximum values can be obtained by a series of points, which reflect the relationship between the heading angle and flight path angle. When the following is satisfied:

$$\sin\gamma = \frac{\cos\psi n_{s2} + \sin\psi n_{s1}}{\sqrt{(\cos\psi n_{s2} + \sin\psi n_{s1})^2 + {n_{s3}}^2}} \quad \ldots(26)$$

the maximum solar energy acquisition is

$$P_{sun} = I_1\sqrt{{n_{s1}}^2 + {n_{s2}}^2 + {n_{s3}}^2} = I_1 \quad \ldots(27)$$

In this case, the normal vector of the wing surface is parallel to the direction of the sunlight. The maximum solar power is obtained without considering other constraints.

The amounts of energy obtained from the wind gradient and solar radiation according to Equations (20) and (25) are related to the heading angle and flight path angle. When the bank angle is optimum, the total energy acquisition can be obtained.

$$P_{in} = -\frac{dV_W}{dh}mV^2\sin\gamma\cos\gamma\sin\psi + I_1\sqrt{(\cos\psi n_{s1} - \sin\psi n_{s2})^2 + (-\sin\gamma(\sin\psi n_{s1} + \cos\psi n_{s2}) + \cos\gamma n_{s3})^2} \quad \ldots(28)$$

The relationship between the total energy acquisition and the flight attitude is shown in Fig. 8 for the following conditions: $dV_W/dh = 0.2s^{-1}$, $V = 21m/s$, nd=180, $t_{mission} = 12{:}00$, $I_1 = 553.8J$:

When the bank angle is unlimited, the maximum energy acquisition rate is closer to the bank angle during dynamic soaring in the wind field. The reason is that the maximum points of the two methods are close to each other, whereas the gradient is smaller near the peak of solar power acquisition.

Equation (28) shows the relationship between the energy acquisition and the flight attitude under ideal conditions. The maximum energy acquisition can be achieved by changing

https://doi.org/10.1017/aer.2020.79 Published online by Cambridge University Press

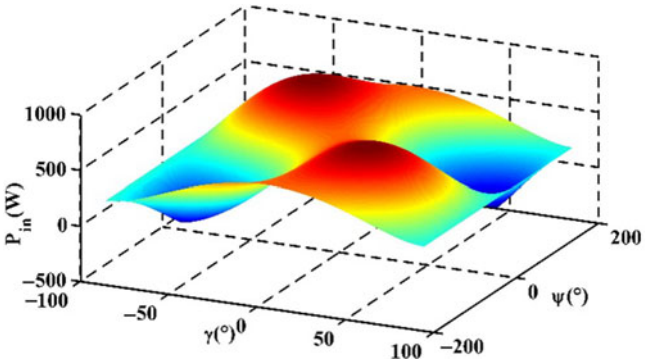

Figure 8. Relationship between total energy acquisition and flight attitude.

the flight attitude. We obtain the partial derivative of Equation (28) and set it equal to 0 to obtain:

$$\frac{\partial P_{in}}{\partial \gamma} = 0 = -\frac{dV_w}{dh} mV^2(\cos^2\gamma - \sin^2\gamma)\sin\psi + I_0 \frac{A \cdot (\cos\psi n_{s1} + \sin\psi n_{s2})\cos\gamma}{\sqrt{A^2 + (\sin\psi n_{s1} - \cos\psi n_{s2})^2}} \quad \ldots(29)$$

$$\frac{\partial P_{in}}{\partial \psi} = 0 = -\frac{dV_w}{dh} mV^2 \cos^2\gamma \sin\gamma \cos\gamma \cos\psi + I_0 \frac{A \sin\gamma(-\sin\psi n_{s1} + \cos\psi n_{s2})}{\sqrt{A^2 + (\sin\psi n_{s1} - \cos\psi n_{s2})^2}} + I_0 \frac{(\sin\psi n_{s1} - \cos\psi n_{s2})(\cos\psi n_{s1} + \sin\psi n_{s2})}{\sqrt{A^2 + (\sin\psi n_{s1} - \cos\psi n_{s2})^2}} \quad \ldots(30)$$

$$A = \sin\gamma(\cos\psi n_{s1} + \sin\psi n_{s2}) + \cos\gamma n_{s3} \quad \ldots(31)$$

The maximum energy acquisition can be obtained when the partial derivative functions are satisfied. The effects of the flight speed and wind gradient on the maximum energy acquisition and the corresponding flight attitude can be determined by changing these factors. The results are shown in Figs 9 and 10.

Figures 9 and 10 show the maximum energy acquisition of a small UAV, which combines two energy acquisition techniques, varying with the flight speed and wind gradient. In Figs 9 and 10, the maximum energy acquisition point together with the points where $\left|P_{in} - P_{in\_\max}\right| <= 0.5W$ corresponding to different flight velocities or wind gradients are shown in the form of a colour gradient surface. The closer to the value of the maximum points, the redder the colour. The coordinate projection on the horizontal plane shows the flight path angle, and the heading angle corresponds to the maximum energy acquisition. The longitudinal coordinate projection represents the value of the energy acquisition, which is convenient for comparing different flight conditions.

https://doi.org/10.1017/aer.2020.79 Published online by Cambridge University Press

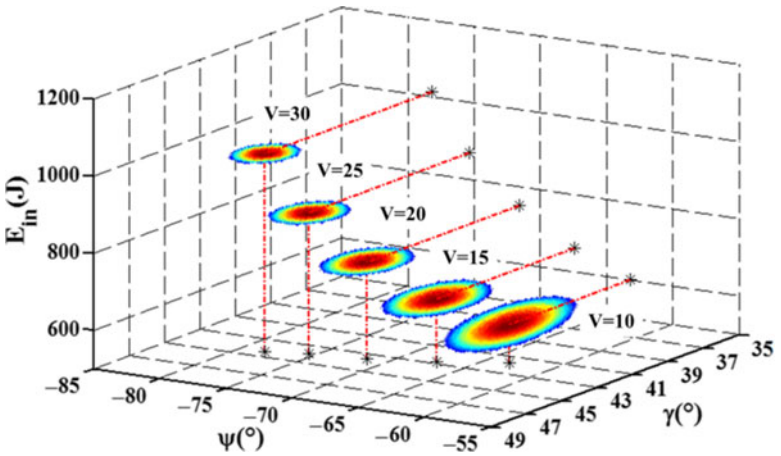

Figure 9. Effect of flight speed on maximum energy acquisition.

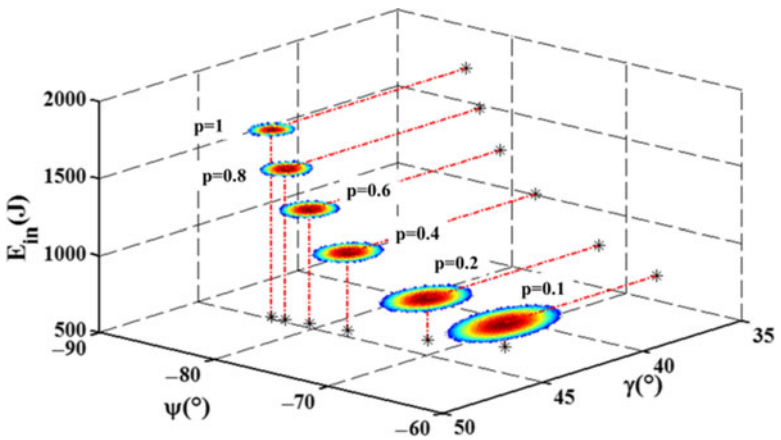

Figure 10. Effect of wind gradient on maximum energy acquisition.

Figure 8 shows that the relationship between the energy acquisition and the flight attitude is symmetrical with respect to the origin centre, therefore, we limit the discussion to $-180° <= \psi = 0°, 0° < \gamma < 90°$ for convenience.

As shown in Fig. 9, as the flight speed increases, the horizontal coordinate projection of the maximum energy acquisition point gradually approaches the maximum wind field energy acquisition point $\psi = -90°, \gamma = 45°$, while the total energy acquisition increases. Equation (28) shows that, as the flight speed increases, the solar energy acquisition remains unchanged, whereas the maximum wind energy acquisition further increases, gradually occupying a dominant position. Similarly, in Fig. 10, it is observed that, as the wind gradient increases, the horizontal coordinate projection of the maximum energy acquisition point gradually approaches the maximum wind field energy acquisition point. This result can be attributed to the increase in the wind gradient, which increases the proportion of wind field energy acquisition.

https://doi.org/10.1017/aer.2020.79 Published online by Cambridge University Press

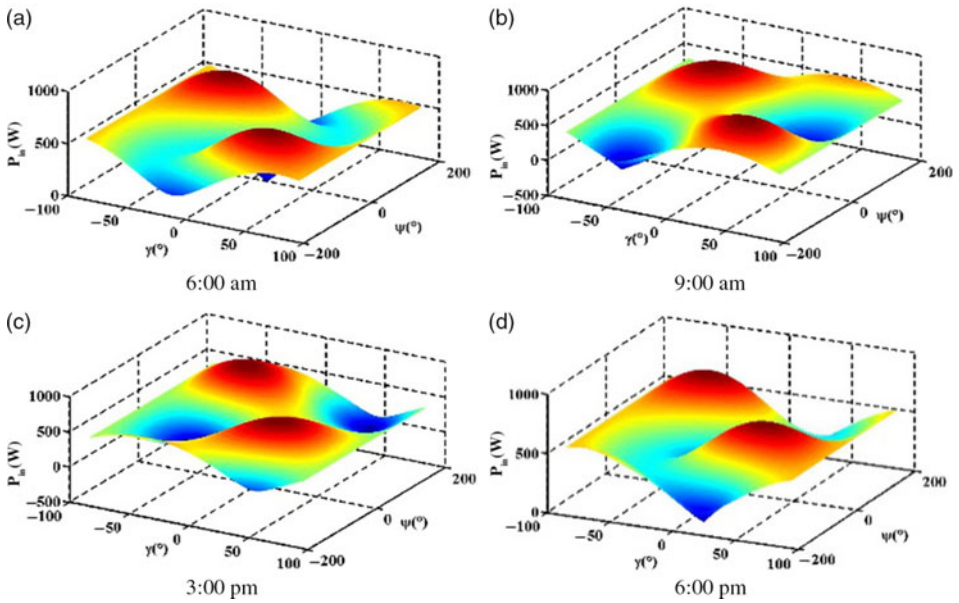

Figure 11. Relation between energy acquisition and flight attitude at different times of day. (a) 6:00 am (b) 9:00 am (c) 3:00 pm (d) 6:00 pm.

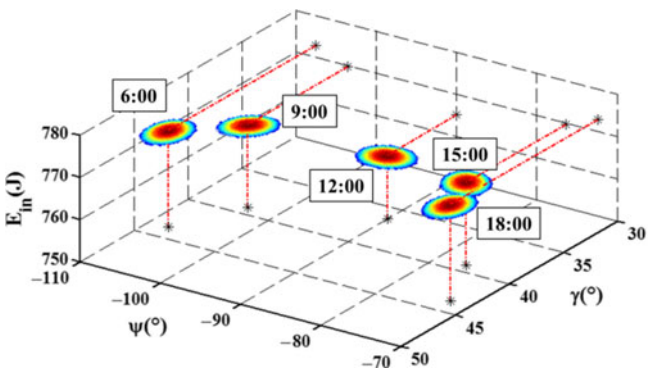

Figure 12. Effect of solar illumination conditions on maximum energy acquisition.

Different values of $\mathbf{n_s} = (n_{s1}, n_{s2}, n_{s3})$ at different times of the day also affect the energy acquisition, as shown in Fig. 11. To obtain the optimal energy acquisition, the small UAV should deflect to the direction of favourable solar energy acquisition and keep the overall trend of upwind climb and downwind dive.

The influence of the solar illumination conditions on the maximum energy acquisition is shown in Fig. 12.

The maximum intensity of the solar illumination varies little at different flight times, but the angle of solar illumination with the ground varies greatly. To maximise the ability to obtain solar energy, it is necessary to change the flight path angle and heading angle based on the illumination conditions and to ensure that the wing of the plane is as perpendicular as possible to the illumination vector. Since the maximum point of solar energy acquisition of the aircraft

https://doi.org/10.1017/aer.2020.79 Published online by Cambridge University Press

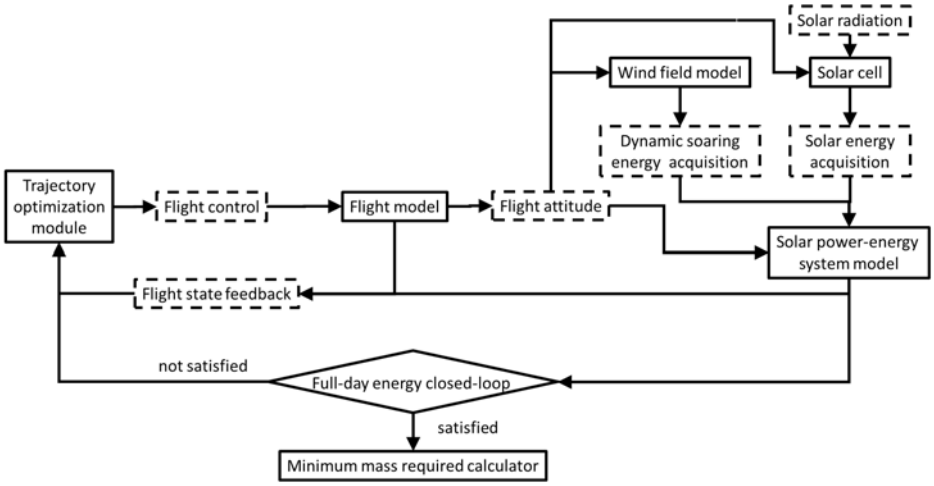

Figure 13. Information flow and structural framework of the trajectory optimisation system.

at 06:00 and 18:00 is closer to the maximum point of wind energy acquisition, the maximum energy acquisition is greater than at 12:00.

Different flight times affect the energy acquisition, but the maximum value is still concentrated near the maximum energy acquisition value of dynamic soaring. Considering the constraints and control requirements regarding the flight trajectory, the attitude variables may not satisfy the requirement for maximum total energy acquisition, but at the optimal attitude, the angle between the solar incident vector and the plane-normal vector of the wing surface should be minimised under the conditions of upwind climbing and downwind diving.

4.0 SIMULATION AND ANALYSIS

A cyclic flight pattern is chosen for the simulation, and a loitering pattern flight path[20] is chosen as the reference flight trajectory. First, the single-cycle circular flight pattern is optimised to obtain the optimal energy acquisition under this condition, and the energy change is analysed to verify the advantages of the dynamic soaring technology in a single cycle for energy acquisition by a small solar UAV. Then, the optimal total energy acquisition at all times of the day is calculated to determine whether the all-day closed-loop energy conditions and the minimum mass of the power energy system can be met. Finally, the minimum mass required for the power energy system under different conditions is calculated to determine the effect of different wind field shapes and sunlight conditions.

4.1 Trajectory optimisation system

The trajectory optimisation system is established based on the model in Section 1 with the parameters of a typical aircraft (Table 1). The information flow and structural framework are shown in Fig. 13. The solar power energy system is an essential module to manage the total energy acquisition and output, including wind and solar energy management.

The trajectory optimisation system is solved with SNOPT.

https://doi.org/10.1017/aer.2020.79 Published online by Cambridge University Press

The objective of the optimisation is to maximise the total energy acquisition to satisfy the all-day closed-loop energy condition:

$$\min J = -E_{sp} = -\int_0^{t_n} \dot{E}_{sp} dt \quad \ldots (32)$$

The model that includes the solar energy model and the dynamic soaring flight model is expressed as follows:

$$\dot{\mathbf{x}}(t) = \mathbf{f}(\mathbf{x}(t), \mathbf{u}(t)) \quad \ldots (33)$$

where $\mathbf{x} = [V, \psi, \gamma, h, x, y]$ is the state vector of the system and $\mathbf{u} = [\mu, C_L, T]$ is the input control vector. The flight trajectory is discretised into M points, and the state vector of each point is determined by the flight control and initial flight state. Therefore, the design variables are

$$\begin{aligned} \mathbf{X} &= [x_{1,1}, ..., x_{6,1}, \\ &\quad u_{1,1}, u_{2,1}, ..., u_{1,M}, u_{2,M}, t_f] \\ &= [\mathbf{x}_1^T, \mathbf{u}_1^T, ..., \mathbf{u}_M^T, t_f] \\ x_{i,m+1} &= x_{i,m} \\ &\quad + (k_{i,m}^1 + 2k_{i,m}^2 + 2k_{i,m}^3 + k_{i,m}^4)\Delta t/6 \end{aligned} \quad \ldots (34)$$

The periodic loitering pattern flight path is selected as the reference optimisation path. The aircraft should be able to return to the initial flight state after completing one cycle to ensure the repeatability of the flight. According to this condition, the following constraints are obtained:

$$\begin{aligned} V(t_f) &= V(t_0) \\ \lambda(t_f) &= \lambda(t_0) \\ h(t_f) &= h(t_0) \\ \psi(t_f) &= \psi(t_0) \\ x(t_f) &= x(t_0) \\ y(t_f) &= y(t_0) \end{aligned} \quad \ldots (35)$$

For reasons of flight safety, the aircraft cannot touch the ground or enter the water during the flight, so there are additional height constraints:

$$h - \frac{1}{2} b \, |\sin(\mu)| \geq h_{\min} \quad \ldots (36)$$

Table 2 presents the optimal initial parameter settings.

4.2 Single-cycle simulation

The flight date is $nd = 180$ in the summer, and the time is $t_{mission} = 18{:}00$ for the single-cycle simulation. At this time, energy can still be obtained from solar radiation, but it is insufficient to provide all the energy required for flight. It is thus necessary to obtain additional energy from the wind field through dynamic soaring. The simulation path results are shown in Fig. 14,

https://doi.org/10.1017/aer.2020.79 Published online by Cambridge University Press

Table 2
Optimal initial parameter settings

Initial parameter	Initial setting
Initial velocity V_1(m/s)	18
Initial heading angle ψ_1(°)	0
Initial flight path angle γ_1(°)	0
Initial coordinates (x_1, y_1, h_1)(m)	(0,0,12)
M	100
Initial flight duration t_{f0}(s)	9
Initial V_R(m/s)	8
Geographical latitude θ_s(°)	45

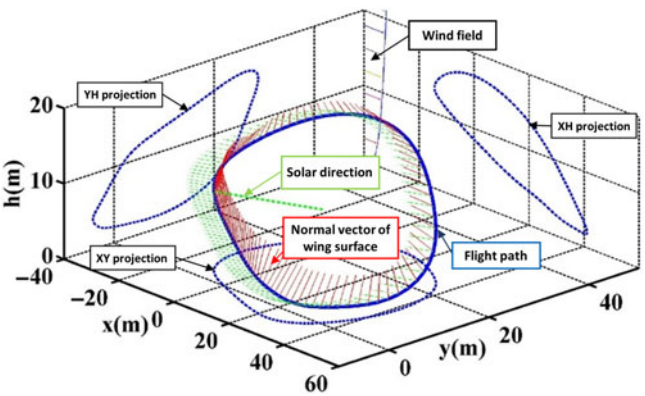

Figure 14. Simulated flight path.

and the flight speed, heading angle and flight path angle during the flight are shown in Fig. 15. Figure 16 shows the changes in the energy components during the flight.

In Fig. 14, the thick solid blue line is the flight trajectory, the dotted blue line is the projection of the flight trajectory on each plane, the dotted green line represents the incident sunlight and the red line represents the normal vector of the main wing plane of the aircraft.

Figure 16 shows that the energy obtained from the wind field is about equal to the solar energy absorbed by the aircraft. At sunset, the aircraft still acquires energy from the sun. While offsetting the energy consumption of the propulsion system and aerodynamic drag, 72.1J of energy is obtained in each circular flight cycle via dynamic soaring. Without the energy from dynamic soaring, the aircraft would lose 320.6J of energy in each circle. The use of dynamic soaring reduces the output energy of the solar power energy system by 32.2%. The total energy budget shows that the combination of solar energy and dynamic soaring provides greater endurance.

4.3 Verification of the all-day closed-loop energy system

4.3.1 72-h flight simulation with a fixed mass

We used the simulation of Section 4.2 and conducted a simulation to optimise the energy acquisition at different times in one day (summer $nd = 180$) to determine whether the

https://doi.org/10.1017/aer.2020.79 Published online by Cambridge University Press

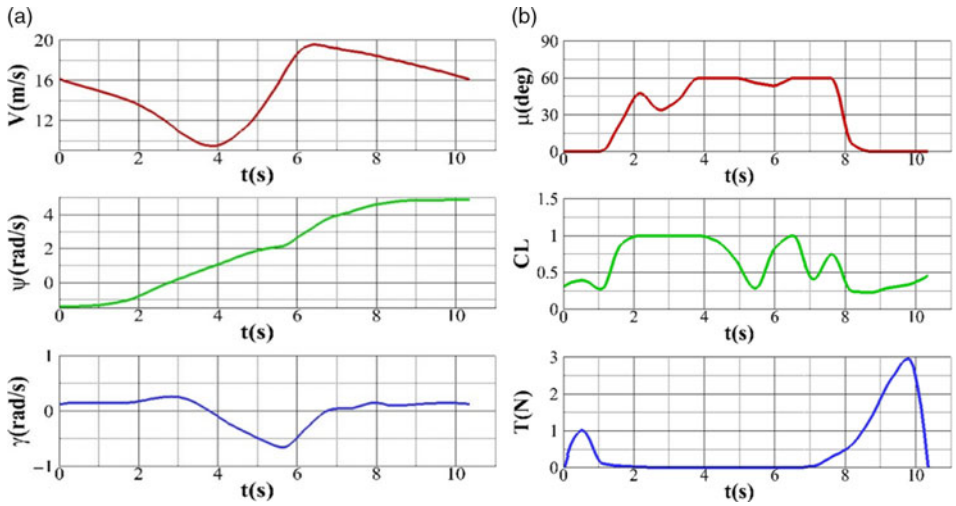

Figure 15. Changes in flight states and control variables.

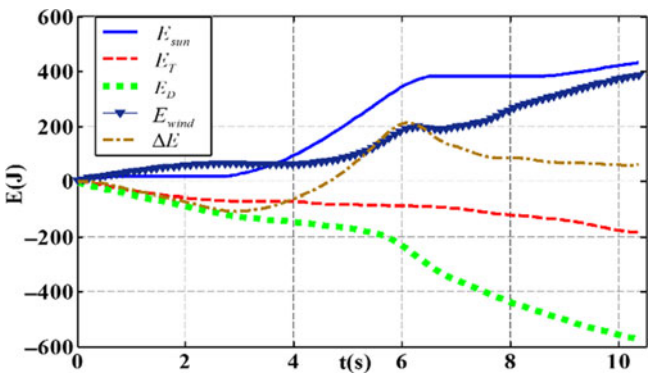

Figure 16. Summary of energy changes.

requirements for the all-day closed-loop energy system were met. The results are shown in Fig. 17.

In Fig. 17, the total power output of the small solar UAV using dynamic soaring is Pbat, and the power output without dynamic soaring is Pbat2. The results show that Pneed, which is the energy that the aircraft needs to maintain flight, is the same during the day and night. Solar energy acquisition during the day supports the energy required for flight, whereas, at night, the UAV relies on dynamic soaring to obtain additional energy from the wind field. Otherwise, it will rely entirely on the energy output of the battery to maintain flight. The use of dynamic soaring at night reduces the battery energy expenditure by 6.7%, thereby greatly improving the endurance of the small UAV.

It can be seen from Fig. 18 that the flight trajectory at each time point follows the overall trend of upwind climb and downwind dive, and according to the different sunlight directions, the flight trajectory deflects to the direction of favourable solar energy acquisition.

https://doi.org/10.1017/aer.2020.79 Published online by Cambridge University Press

Table 3
Simulation results of the solar power energy system

	E_{charge}	m_{bat}	m_T	m_{sp}
DS	48.6Wh	0.355kg	0.104kg	0.659kg
no_DS	1066.36Wh	7.789kg	0.478kg	8.467kg

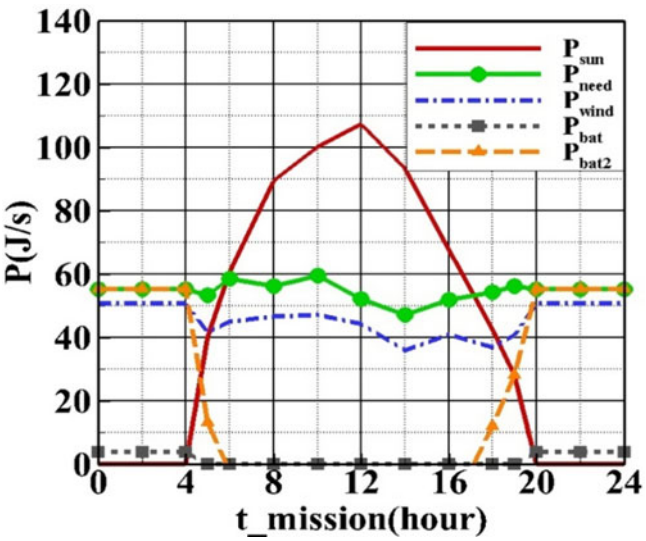

Figure 17. Power variation in the all-day closed-loop energy system.

Assuming that the mass of the power system is 40% of the total mass of the aircraft (5.443kg), i.e., 2.17kg, the battery energy storage is 597Wh. A 72-h flight simulation is conducted, and the results are shown in Fig. 19.

The results show that the energy consumption during dynamic soaring (*DS* in Fig. 19) is much lower than that without dynamic soaring (*no_DS* in Fig. 19); the *DS* curve shows that the use of dynamic soaring meets the requirements for the all-day closed-loop energy system, and 72h of continuous flight is achieved. Without dynamic soaring, the energy reserve would be exhausted after 26h. The slope of the *DS* curve during the day is greater than that of the *no_DS* curve, which indicates that dynamic soaring is conducive to daytime energy acquisition.

4.3.2 Simulation of the solar power energy system with the minimum mass

The 72-h flight simulations with *DS* and *no_DS* are performed to calculate the minimum mass of the solar power energy system that is required to ensure all-day closed-loop energy conditions. The minimum mass required to maintain a closed-loop energy system is shown in Table 3. The energy change of the solar power energy system in 72h starting at 0:00 is shown in Fig. 20.

Table 3 shows that the total mass of the solar power energy system needed to maintain 72h of uninterrupted flight for the small solar UAV using dynamic soaring (*DS*) is 0.659kg;

https://doi.org/10.1017/aer.2020.79 Published online by Cambridge University Press

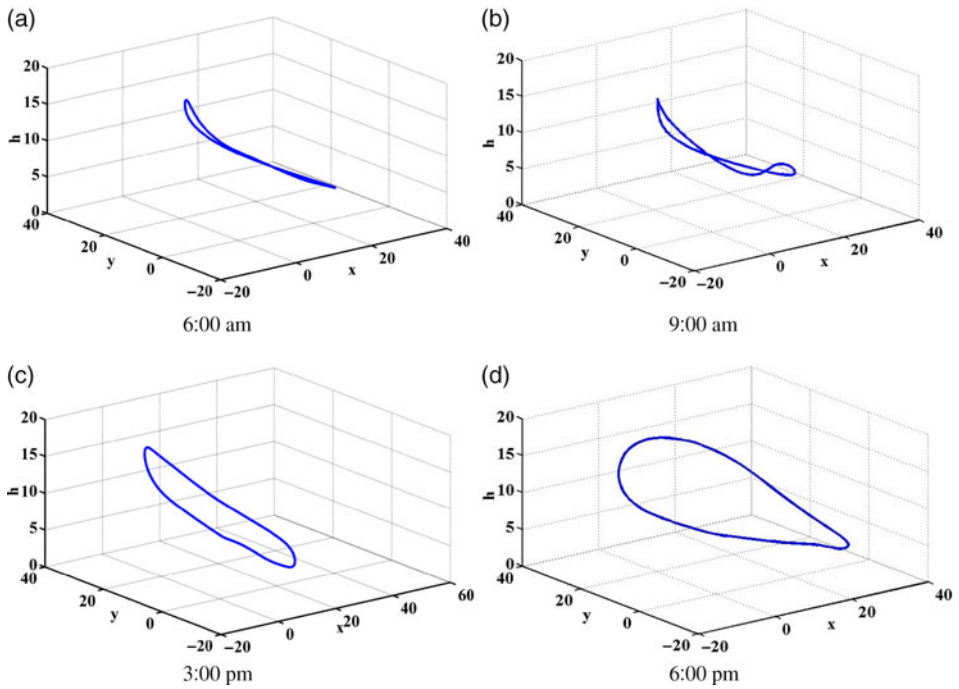

Figure 18. Flight trajectories at different times of the day. (a) 6:00 am (b) 9:00 am (c) 3:00 pm (d) 6:00 pm

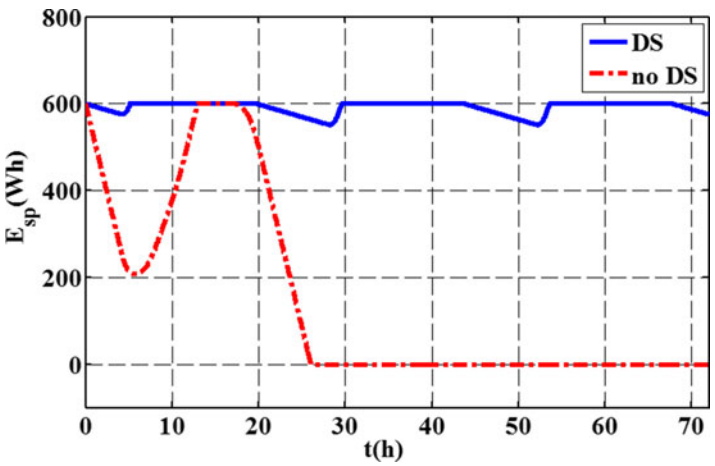

Figure 19. Energy changes during the 72-h flight simulation.

this mass is only 7.8% of the mass of the system that does not use dynamic soaring. The minimum mass of the solar power energy system required for the UAV without dynamic soaring (*no_DS*) is 5.443kg, which is larger than the total mass of the UAV, indicating that this is not a feasible solution. As shown in Fig. 20, the energy of the *DS* energy system exhibits changes during the 24-h cycle, demonstrating that the system is an all-day closed-loop energy system, and the UAV is able to fly continuously day and night. In contrast, the

https://doi.org/10.1017/aer.2020.79 Published online by Cambridge University Press

Table 4
Influence of different values of p on the mass of the energy system

	E_{charge}	m_{bat}	m_T	m_{sp}
$p=0.25$	48.6Wh	0.355kg	0.104kg	0.659kg
$p=0.6$	20.1Wh	0.147kg	0.007kg	0.354kg
$p=1$	0Wh	0kg	0kg	0kg

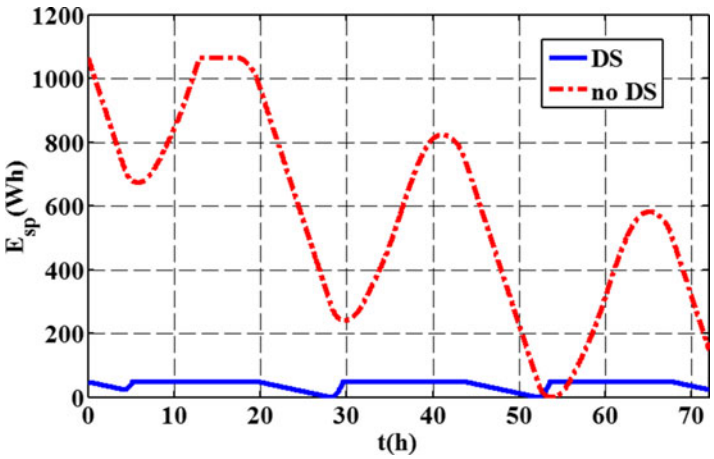

Figure 20. Energy change results without mass constraints.

no_DS system has insufficient energy at night to maintain flight and is not an all-day closed-loop energy system. The simulation results show that dynamic soaring significantly reduces the energy consumption of the small solar UAV, increases its endurance and results in an all-day closed-loop energy system.

4.4 Influence of the wind field

Equation (14) shows that the wind field representative velocity V_R and the wind field power-law exponent p have strong effects on the ability to obtain energy from dynamic soaring. Since dynamic soaring is a key energy source, it is important to assess the effect of the wind field on the energy system. The effects of the wind field are assessed using a 72-h simulation of the solar power energy system with a minimum mass. The results are shown in Fig. 21 and Table 4.

The wind field model shows that, the greater the wind field power-law exponent p, the larger the wind gradient. Equation (28) shows that a larger wind gradient allows for more energy extraction from the wind field, resulting in less energy loss at night and faster energy replenishment in the daytime. Therefore, the mass requirement of the system is lower. When $p=1$, the aircraft is powered only by the energy obtained from dynamic soaring, and there is no need for a battery to maintain a closed-loop energy system.

As shown in Fig. 22 and Table 5, as the wind field representative velocity V_R increases, less battery energy is used at night, and the minimum mass of the energy system decreases. As V_R decreases, the minimum mass increases significantly. When $V_R=2$, the minimum mass

https://doi.org/10.1017/aer.2020.79 Published online by Cambridge University Press

Table 5
Influence of different value of V_R on the mass of the energy system

	E_{charge}	m_{bat}	m_T	m_{sp}
$V_R = 8$	48.6Wh	0.355kg	0.104kg	0.659kg
$V_R = 5$	219.6Wh	1.605kg	0.245kg	2.05kg
$V_R = 2$	327.9Wh	2.397kg	0.306kg	2.903kg

Table 6
Influence of different flight dates *nd* on the mass of the energy system

	E_{charge}	m_{bat}	m_T	m_{sp}
$nd = 0$	108.5Wh	0.793kg	0.122kg	1.115kg
$nd = 90$	74.3Wh	0.543kg	0.130kg	0.873kg
$nd = 180$	48.6Wh	0.355kg	0.104kg	0.659kg
$nd = 270$	77.3Wh	0.565kg	0.113kg	0.878kg

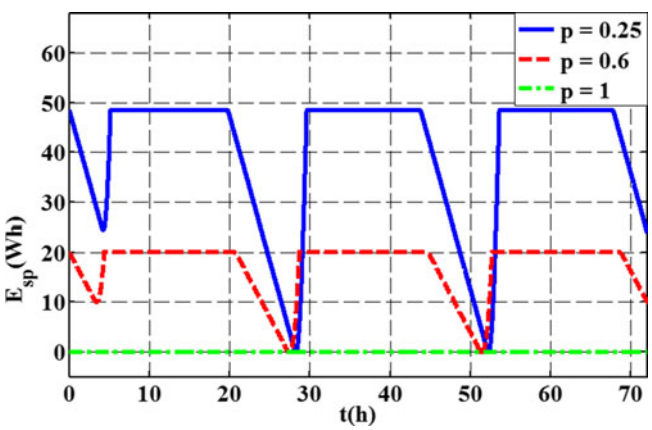

Figure 21. Simulation results showing the influence of different values of p.

exceeds 50% of the total mass of the UAV, which poses a dangerous load on the aircraft, but the minimum mass is still lower than for the system that does not use dynamic soaring.

In summary, larger p and V_R values enable the aircraft to obtain more energy from the wind field by using dynamic soaring and the ability to achieve closed-loop energy conditions.

4.5 Influence of solar conditions

Solar conditions affect the efficiency of energy acquisition. The solar elevation angle and radiation intensity depend on the flight date. The simulation results showing the influence of different flight dates on the minimum mass of the power energy system are shown in Fig. 23 and Table 6.

In the winter ($nd = 0$), the days are short while the nights are long. The efficiency of solar energy acquisition is low, and more battery energy is used; therefore, a heavier battery pack

https://doi.org/10.1017/aer.2020.79 Published online by Cambridge University Press

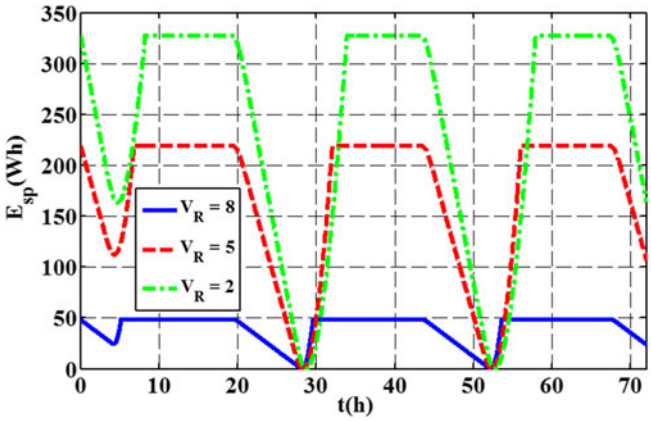

Figure 22. Simulation results showing the influence of different values of V_R.

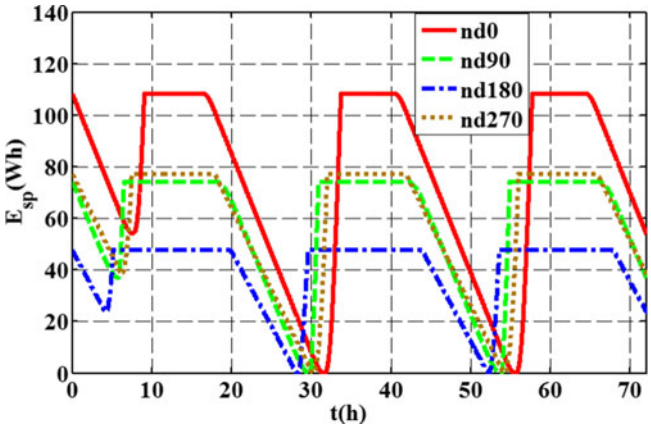

Figure 23. Simulation results showing the influence of different flight dates *nd*.

is required to provide energy. In the summer ($nd = 180$), a lighter battery pack can be used; the battery requirements are similar in the spring and autumn. The results show that stronger solar illumination has energy and load advantages. The slopes of the curves are the same, indicating that the energy obtained from dynamic soaring is the same in all seasons.

5.0 CONCLUSION

We investigated the conditions to achieve a closed-loop energy system in a small solar UAV by exploiting dynamic soaring. The method to maximise the energy acquisition from dynamic soaring and solar radiation during the day and night is analysed. The following conclusions can be drawn:

1. The key factors that influence the ability to achieve a closed-loop energy system in the small solar UAV are the battery weight and the energy capacity. We determined the minimum mass of the energy system that is required to achieve a closed-loop energy system.

https://doi.org/10.1017/aer.2020.79 Published online by Cambridge University Press

The flight speed and flight attitude angles have significant effects on the efficiency of energy acquisition.

2. Dynamic soaring enables the UAV to obtain additional energy from the wind field and reduce energy consumption, especially at night. The simulation results show that the use of dynamic soaring reduces the energy consumption of the UAV energy system by 32.3%. The 72-h flight simulation shows that dynamic soaring results in closed-loop energy conditions, and the minimum mass of the energy system is only 6.7% of the mass of a system that does not use dynamic soaring. Dynamic soaring greatly reduces the energy consumption and significantly improves the endurance of the UAV.
3. The influence of the wind field shape and solar conditions on the ability of the UAV to achieve all-day closed-loop energy conditions are investigated to lay a foundation for future research on the combination of dynamic soaring and solar power in small UAVs. A larger wind field intensity index p and wind velocity V_R enable the UAV to obtain more energy from the wind field. The flight date affects the efficiency of the solar energy acquisition and energy consumption at night but has little effect on the ability to obtain energy from dynamic soaring.

REFERENCES

1. LUO, D., RONGZENG, X. and HAIBIN, D. A guidance law for UAV autonomous aerial refueling based on the iterative computation method, *Chin J Aeronaut*, 2014, **27**, (4), pp 875–83.
2. OUYANG, J., ZHUANG, Y., LIN, M. and LIU, J. Optimization of beamforming and path planning for UAV-assisted wireless relay networks, *Chin J Aeronaut*, 2014, **2**, pp 313–20.
3. NG, T.T.H. and LENG, G.S.B. Design of small-scale quadrotor unmanned air vehicles using genetic algorithms, *Proc Inst Mech Eng G: J Aerosp Eng*, 2007, **221**, (5), pp 893–905.
4. HARASANI, W., ARAI, N., KHALID, M. and FUKUDA, K. Initial conceptual design and wing aerodynamic analysis of a solar power-based UAV, *Aeronaut J*, 2014, **118**, (1203), pp 540–54.
5. YANG, W. and WEI, L. Searching and tracking ground target UAV flight control system design, *J Beijing Univ Aeronaut Astronautics*, 2010, **36**, (10), pp 1252–55.
6. Unmanned Aircraft Systems Road Map 2005–2030, Unite States Department of Defense, July 2005, pp. 51.
7. NOTH, A. Design of solar powered airplanes for continuous flight, PhD Thesis, ETH Zürich, Zürich, 2008.
8. LANGELAAN, J.W. and ROY, N. Enabling new missions for robotic aircraft, *Science*, 2009, **326**, pp 1642–4.
9. KLESH, A.T. and KABAMBA, P.T. *Energy-Optimal Path Panning for Solar-Powered Aircraft in Level Flight, AIAA-2007-6655*, AIAA, 2007, Reston.
10. SINEGLAZOV, V.M. and KARABETSKY, D.P. Energy system design of solar aircraft, Actual Problems of Unmanned Air Vehicles Developments, IEEE, 2014.
11. SINEGLAZOV, V.M. and KARABETSKY, D.P. Flying wing design for solar rechargeable aircraft, IEEE International Conference Actual Problems of Unmanned Air Vehicles Developments, IEEE, 2014.
12. SPANGELO, S.C., GILBERTY, E.G. and KLESHZ, A.T. *Periodic Energy-Optimal Path Planning for Solar-Powered Aircraft, AIAA-2009-6016*, AIAA, 2009, Reston.
13. SPANGELO, S.C. and GILBERT, E.G. Power optimization of solar-powered aircraft with specified closed ground tracks, *J Aircr*, 2013, **50**, (1), pp 232–8.
14. CHANG, M., ZHOU, Z. and ZHENG, Z.. Flight principles of solar-powered airplane and sensitivity analysis of its conceptual parameter, *J Northwestern Polytech Univ*, 2010, **28**, (5), pp 792–6.
15. CHANG, M., ZHOU, Z. and LI, Y. An effective theoretical analysis of persistent flight altitudes of solar-powered airplanes, *J Northwestern Polytech Univ*, 2012, **30**, (4), pp 541–6.
16. BRANDT, S.A. and GILLIAMT, F.T. Design analysis methodology for solar-powered aircraft, *J Aircr*, 1995, **32**, (4), pp 703–709.

https://doi.org/10.1017/aer.2020.79 Published online by Cambridge University Press

17. MA, D., BAO, W. and QIAO, Y. Study of flight path for solar-powered aircraft based on gravity energy reservation, *Acta Aeronaut Astron Sin*, 2014, **35**, (2), pp 408–416.
18. RAYLEIGH, J.W.S. The soaring of birds, *Nature*, 1883, **27**, pp 46–58.
19. SACHS, G., TRAUGOTT, J. and NESTEROVA, A.P. Flying at no mechanical energy cost: disclosing the secret of wandering albatrosses, *Plos ONE*, 2012, **7**, (9), e41449.
20. ZHAO, Y. Optimal patterns of glider dynamic soaring, *Optim Control Appl Methods*, 2004, **25**, pp 67–89.
21. ZHAO, Y. and QI, Y.C. Minimum fuel powered dynamic soaring of unmanned aerial vehicles utilizing wind gradients, *Optim Control Appl Methods*, 2004, **25**, (5), pp 211–33.
22. SACHS, G. Minimum shear wind strength required for dynamic soaring of albatrosses, *IBIS*, 2005, **147**, pp 1–10.
23. SACHS, G. and BUSSOTTI, P. Application of optimal control theory to dynamic soaring of seabirds, *Variational Analysis and Applications*, 2005, **79**, pp 975–94.
24. DEITTERT, M., RICHARDS, A. and TOOMER, C.A. Engineless unmanned aerial vehicle propulsion by dynamic soaring, *J Guid Control Dyn*, 2009, **32**, (5), pp 1446–57.
25. LIU, D.N., HOU, Z.X. and GUO, Z. Optimal patterns of dynamic soaring with a small unmanned aerial vehicle, *Proc Inst Mech Eng G J Aerosp Eng*, 2017, **231**, (9), pp 1593–608.
26. ZHU, B. and HOU, Z. Energy transformation in dynamic soaring of unmanned aerial vehicles, *J Natl Univ Defense Technol*, 2015, **37**, (1), pp 78–83.
27. GAO, X. Research on High-Altitude Long-Endurance Flight of Solar-powered Aircraft based on Gravitational Potential and Wind Shear, PhD Thesis, National University of Defense Technology, China, 2014.
28. ZHU, W., LI, J. and XU, Y. Optimum attitude planning of near-space solar powered airship, *Aerosp Sci Technol*, 2019, **84**, pp 291–305.
29. JUN, L., JUN, L. and YUXIN, L. An approach for estimating perpetual endurance of the stratospheric solar-powered platform, *Aerosp Sci Technol*, 2018, **79**, pp 118–30.

https://doi.org/10.1017/aer.2020.79 Published online by Cambridge University Press